

# Book chapter

*by Ian Yulianti*

---

**Submission date:** 09-Apr-2023 09:13PM (UTC+0700)

**Submission ID:** 2059548860

**File name:** Chapter\_8\_final.docx (830.81K)

**Word count:** 3084

**Character count:** 17221

## CHAPTER 9

# Plastic Optical Fiber Mach-Zehnder Interferometer for Intensity-Based Refractive Index Sensor

- 1.1 Introduction 1
- 1.2 Plastic Optical Fiber Mach-Zehnder Interferometer 3
- 1.3 Method 5
- 1.4 Results and Discussions 6
  - 1.4.1 Sensitivity and Linearity 8
  - 1.4.2 Hysteresis and Accuracy 12
- 1.5 Conclusion 16

### 1.1 INTRODUCTION

11

Optical fiber sensors have attracted attention due to their advantages, such as resistance to electromagnetic interference, light in weight, small in size, small transmission attenuation, fast response, flexible geometry, and large bandwidth. Fiber optic sensors can be applied in high voltage, high temperature, or corrosive environments. Moreover, the optical fiber sensor can be implemented for remote monitoring. Fiber optic sensors has been proposed for various measurements, such as strain (Chen et al. 2021), displacement (Ghaffar et al. 2021), refractive index (Zheng et al. 2021), temperature (Su et al. 2021), pressure (X. Li et al. 2020) and biosensor (Xu, Xiong, and Yan 2021).

Refractive index is one of the important parameters in many applications such as biomedical, biochemical, food and environmental industries. Various methods have been developed to

*Book Title (Italic)*

**Comment**  
have attract  
resistance t  
small in siz  
flexible geo

20 design fiber optic refractive index sensor, such as surface plasmon resonance (SPR) method (W. Li et al. 2020; Zhang et al. 2018), Fabry-Perot interferometer (Huang et al. 2020), evanescent wave (Samavati et al. 2019) and Mach-Zehnder interferometer (MZI) (Wu et al. 2021). Among those methods, MZI has advantages of good linearity, low cost, compact size and simple fabrication process.

4 The principle of MZI refractive index sensor is by observing the wavelength shift of the output spectrum due to the change of the environmental refractive index. MZI refractive index sensors have been reported using single mode silica optical fiber (SMF) by implementing various structures. Bhardwaj and Singh (2016) fabricated MZI in SMF by cascading two tapers using a fusion splicer. It was obtained that the sensitivity was 380nm/RIU. Melo et al. (2016) obtained refractive index sensor with sensitivity of 1307nm/RIU by using a Mach-Zehnder interferometer coated with hafnium oxide. Other SMF-based MZI was proposed by Wang et al (2016). The MZI was constructed from photonic crystal fiber (PCF) spliced in between two segments of SMF resulting in sensitivity of 260.8nm/RIU. It is clear that the SMF-MZI has advantage of high sensitivity. Moreover, it also offers high reproducibility and large operational range. However, the SMF MZI has low mechanical strength. Jasim et al. (2014) has proposed MZI using graded-index (GI) plastic optical fiber (POF) by forming two tapers using heat-and-pull technique. The advantages of POF are that it has higher dimension and high mechanical strength than the SMF. Nevertheless, it has drawback of low sensitivity. It was found that the proposed GI-POF based MZI has a sensitivity of only 3.44nm/RIU.

Beside exploiting the wavelength shift, measurement using MZI can also be conducted by observing the change of the output intensity. The advantage of adopting MZI for intensity modulation-based sensor is that it can improve the sensitivity. Moreover, by using MZI, the intensity measurement can be performed at two different

Comment  
obtained a  
1307nm/RI  
coated with

Comment

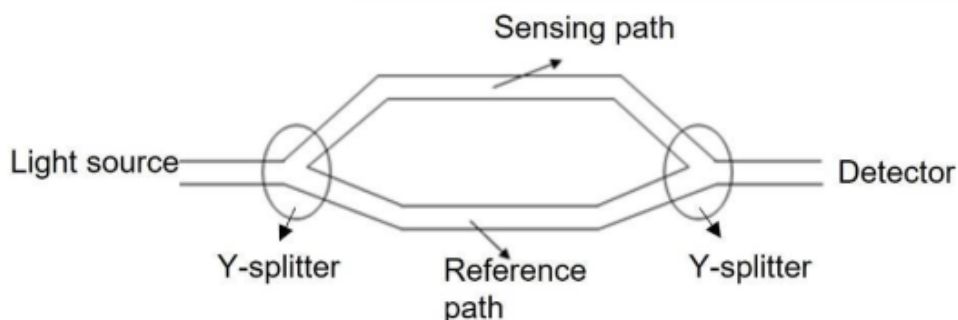
wavelengths. Dual-wavelength measurement method could be applied to overcome the drawback of the intensity-based sensor which is strongly influenced by intensity fluctuations which further limits its accuracy (Tapetado et al. 2014). Therefore, in this work, we proposed an intensity-based POF-MZI sensor for refractive index sensor by implementing a dual-wavelength measurement method. Characterization and analyses were conducted in terms of sensitivity, linearity, hysteresis and accuracy.

Comment  
work, we p  
refractive i  
measureme

## 1.2 PLASTIC OPTICAL FIBER MACH-ZEHNDER INTERFEROMETER

MZI sensor is a phase modulation sensor using a two-beam interferometer. The input light is separated into two parts which are the reference path and the sensing path, as shown in Figure 1.1. The reference path is the path that covered with an insulated shield, while the sensing path is the sensing area exposed to external factors such as temperature, refractive index, and strain. After being separated for certain distance, the reference path and the sensing part are then recombined. Once the light is recombined, interference occurs due to the phase difference.

Comment



Comment  
the path co  
path is the s  
temperature  
separated fo  
sensing par  
recombined

Comment

**Figure 1.1** Structure of basic Mach-Zehnder Interferometer

Intrinsic MZI could be realized using POF by forming two tapers separated at certain distance. POF has advantage of having large core diameter which is around 1 mm. This large diameter makes POF

more durable and flexible than fiber glass. One of the main disadvantages of POF is it has a much higher power loss compared to silica optical fiber. Due to its high power loss, POF is not suitable for long distance communication system. Instead, POF is widely used in optical sensor applications.

MZI structure using POF is shown in Figure 1.2. The two tapers are separated by a distance  $L$ . The POF portion is heated and stretched to form taper. Coherent light source as sensor input propagates in the core mode. When the light pass through the first taper, the light split into the cladding while the rest continues to propagate in the core. The light that propagates inside the cladding has difference phase with that propagates inside the core due to the difference of the refractive index. The light is then recombined at the second taper. The recombined light intensity is defined by (Jasim et al. 2014)

$$I_{out} = I_1 + I_2 + 2\sqrt{I_1 I_2} \cos \Delta\phi \quad (1.1)$$

where  $I_1$ ,  $I_2$ ,  $\Delta\phi$  are the intensity of light propagates at core, the intensity of light propagates at cladding and the phase difference between core mode and cladding modes, respectively. The phase difference depends on the effective refractive index of the core ( $n_{core}$ ), and effective refractive index of the cladding ( $n_{clad}$ ) and also the wavelength of the light ( $\lambda$ ) as defined by

$$\Delta\phi = \frac{2\pi}{\lambda} \Delta N_{eff} L \quad (1.2)$$

where  $\Delta N_{eff} = n_{clad} - n_{core}$  and  $L$  is the interferometer length. From equation (1.2), it is shown that the intensity of the transmitted light at certain wavelength highly depends on the effective refractive index of the core and the cladding. Since the cladding exposed to the environment, then its effective refractive index value change as the environment refractive index changes. Therefore, by observing the change of intensity at certain wavelength, the environment refractive index can be determined. To eliminate the fluctuation of

the intensity due to other factors that commonly occurs in intensity-based sensor, we proposed dual-wavelength method.

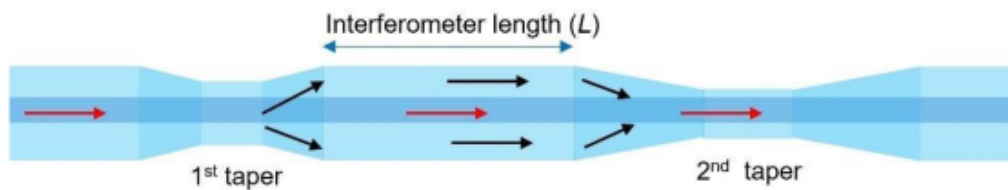


**Figure 1.2** Intrinsic MZI structure

### 1.3 METHOD

The intrinsic MZI was fabricated using step index (SI) POF with core diameter of  $980\mu\text{m}$  (CC2-1000, Sichuan Huiyuan Plastic Optical Fiber Co., Ltd.). The core material and cladding material refractive index are 1.49 and 1.41, respectively. The core material of the POF is PMMA, while the cladding material is fluorinated polymer. The first step of the MZI fabrication was removing the polyethylene jacket of the POF using fiber stripper. To remove any excess dirt, the POF was then cleaned using alcohol. The two ends of the POF were attached to SMA 905 connector (Industrial Fiber Optics, Inc) after polished them using fiber optic sandpaper. Tapers were obtained by heating the POF using solder at temperature of  $80^{\circ}\text{C}$  (Jasim et al. 2014). The distance of the two tapers is 1 cm. Measurement of the taper waist diameters were done by using CCD-optical microscope.

The sensor response to the environment refractive index change was characterized by immersing the MZI-POF in glucose solution. The glucose concentration was varied with an increment of 2% in the range of 0% to 12% at room temperature which correspond to the refractive index of 1.3330 to 1.3547 (measured using ABBE refractometer). Light was launched at the one end of the POF, so that it propagates through the MZI. As a light source, a light emitting diode (LED) having wavelength of 430nm and bandwidth

of 80nm was used. At the other end, the POF was connected to a spectrometer (Ocean Optics UV-VIS), so that the output spectrum could be recorded. The characterization set-up is shown in Figure 1.3.

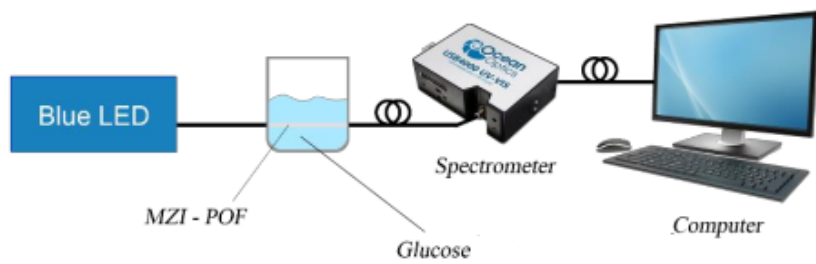
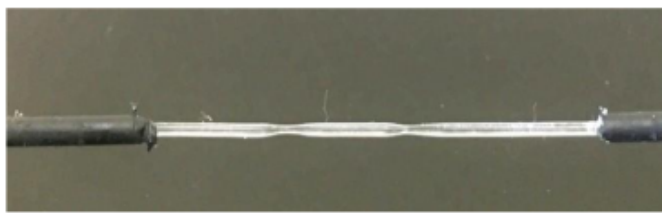


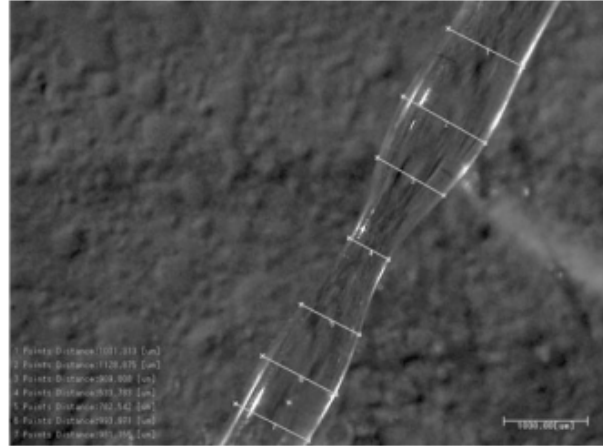
**Figure 1.3** Equipment set up for characterization of the sensor

#### 1.4 RESULTS AND DISCUSSIONS

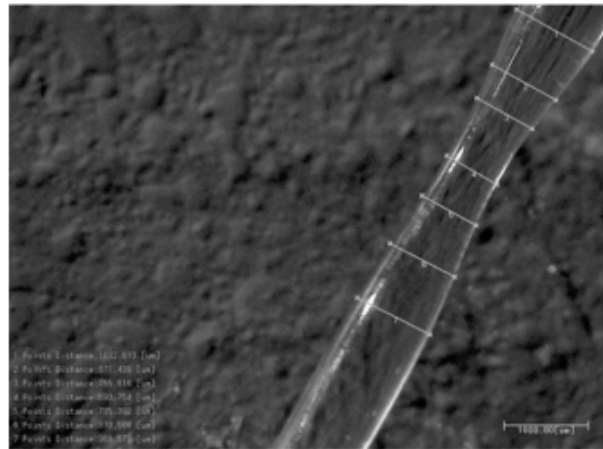
The fabricated MZI is shown in Figure 1.4 (a) and the images obtained from CCD microscope are shown in Figure 1.4 (b) and Figure 1.4(c). It is shown that two tapers have been formed on the POF. The first taper and the second taper diameters are 533.783 and 690.74  $\mu\text{m}$  respectively. It is shown that the first taper is sharper than the second taper to allow excitation of cladding modes. Meanwhile, the smooth second taper was designed to reduce loss when the light recombine.



(a)



(b)



(c)

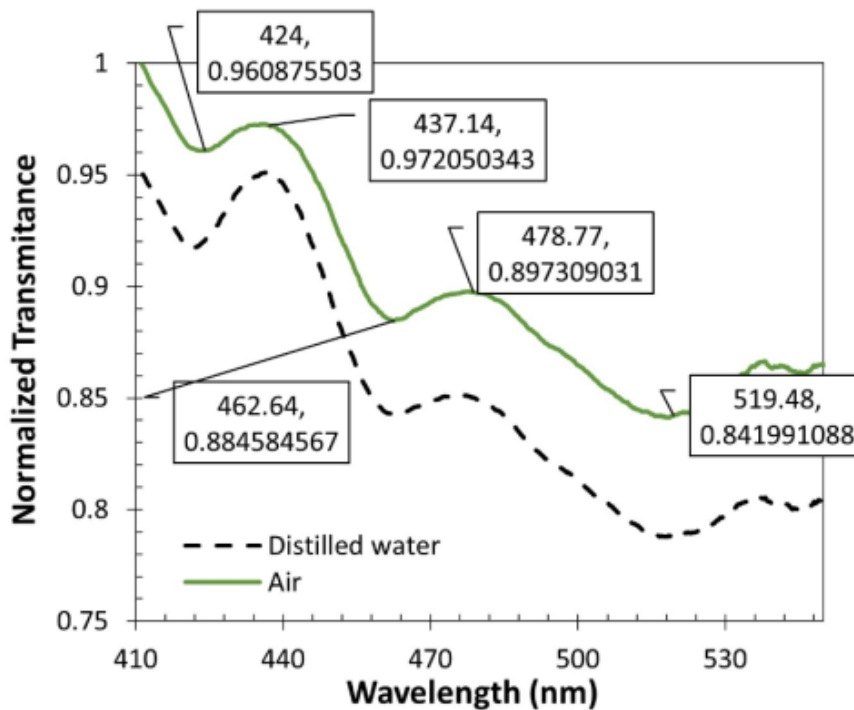
**Figure 1.4** (a) The fabricated MZI, (b) microscope image of the first taper and (c) microscope image of the second taper

The transmittance of the MZI in the air and in distilled water are shown in Figure 1.5. It is observed that the spectra show interference pattern with three dips and two peaks. The dips occurred at wavelength of 424 nm ( $\lambda_1$ ), 462.64 nm ( $\lambda_3$ ), and 519.48 nm ( $\lambda_5$ ), whereas the peaks occurred at 437.14 nm ( $\lambda_2$ ) and 478.77 nm ( $\lambda_4$ ). It is also shown that the transmittances in distilled water are lower than that in the air. The lower transmittance occurred due to the influence of the refractive index of the distilled water which



19

is higher than the refractive index of the air. This result agrees with the Snell's law that states that higher cladding refractive index results in higher critical angle. Hence, more light will be refracted to the cladding region which further causes the decrease of the transmittance. The same results also obtained when the MZI was characterized in various refractive index solutions, as shown in Figure 1.6. As the refractive index increased, the transmittance decreased for all wavelength range.



22

**Figure 1.5** Spectra of the MZI in the air and in distilled water.

#### 1.4.1 Sensitivity and Linearity

Dual-wavelength method was realized by taking the transmittance ratio of two wavelengths. For this purpose, the above-mentioned wavelength of the dips and the wavelength of peaks were used. Ten wavelength pairs were compared and analyzed to obtain the best performance in terms of sensitivity and linearity. The wavelength

pairs were  $\lambda_1/\lambda_2$ ,  $\lambda_1/\lambda_3$ ,  $\lambda_2/\lambda_3$ ,  $\lambda_1/\lambda_4$ ,  $\lambda_2/\lambda_4$ ,  $\lambda_3/\lambda_4$ ,  $\lambda_1/\lambda_5$ ,  $\lambda_2/\lambda_5$ ,  $\lambda_3/\lambda_5$  and  $\lambda_4/\lambda_5$ . The transmittance ratios were calculated from the spectra of the MZI output in various refractive index solutions which is shown in Figure 1.6.

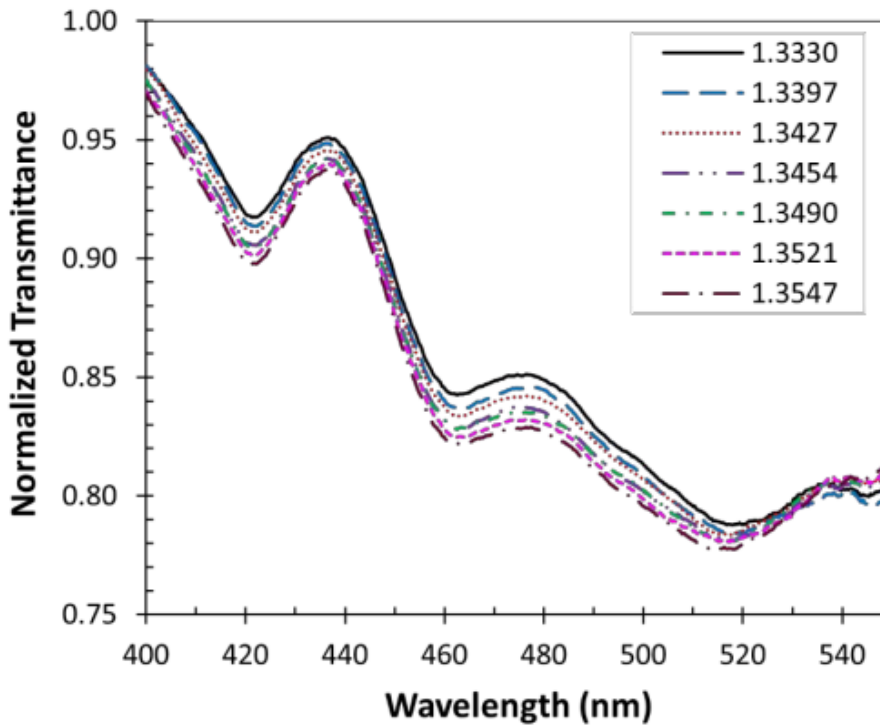


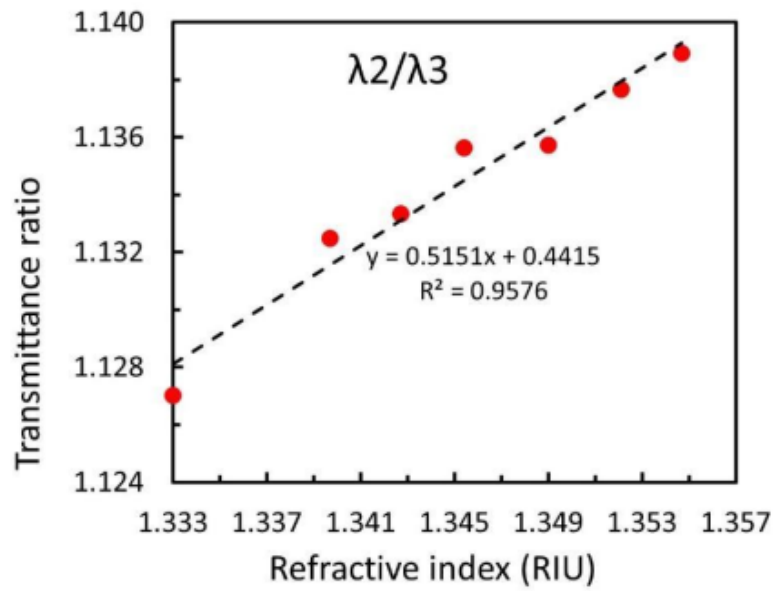
**Figure 1.6** Spectra of the MZI output in various refractive index solutions.

To obtain the refractive index sensitivity and the linearity response of the MZI, the calculated transmittance ratios were plotted against the refractive index values. The results showed that from all wavelength pairs, there are six pairs that have good linearity, as indicated by correlation factor of above 0.9, which arranged from the highest are  $\lambda_2/\lambda_4$ ,  $\lambda_1/\lambda_2$ ,  $\lambda_2/\lambda_3$ ,  $\lambda_1/\lambda_4$ ,  $\lambda_3/\lambda_5$ , and  $\lambda_4/\lambda_5$  as shown in Table 1.1. The highest linearity was 0.9979 which is occurred at wavelength of  $\lambda_2/\lambda_4$  with sensitivity of 0.6336/refractive index unit (RIU). Meanwhile, in terms of sensitivity, the highest six wavelength pairs are  $\lambda_4/\lambda_5$ ,  $\lambda_3/\lambda_5$ ,  $\lambda_2/\lambda_4$ ,  $\lambda_2/\lambda_3$ ,  $\lambda_1/\lambda_4$  and  $\lambda_1/\lambda_2$ .

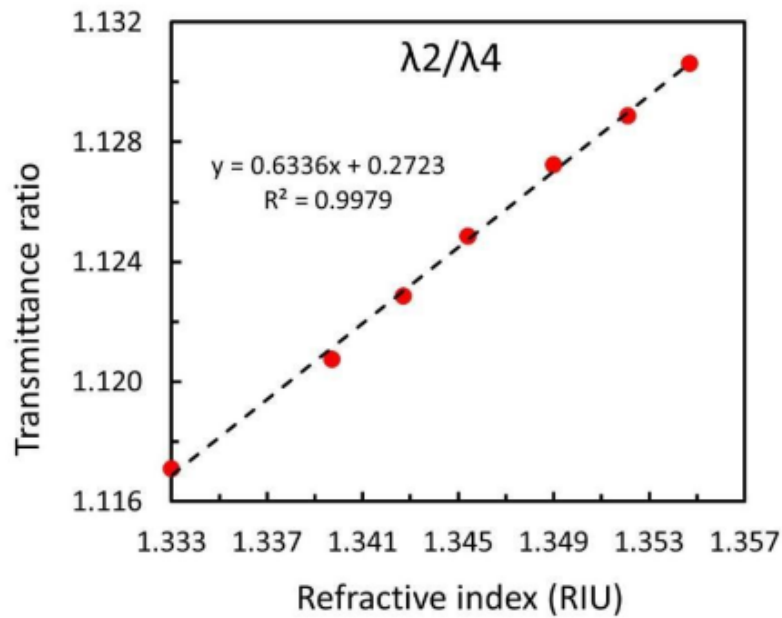
**Table 1.1** Sensitivity and linearity of the MZI of various wavelength pairs

Wavelength pairs	Absolute Sensitivity values (/RIU)	Correlation factor ( $R^2$ )
$L_1/L_2$	<b>0.2877</b>	<b>0.9579</b>
$L_1/L_3$	0.1790	0.5873
$\lambda_2/\lambda_3$	<b>0.5151</b>	<b>0.9576</b>
$\lambda_1/\lambda_4$	<b>0.2880</b>	<b>0.9511</b>
$\lambda_2/\lambda_4$	<b>0.6336</b>	<b>0.9979</b>
$\lambda_3/\lambda_4$	0.1083	0.4886
$\lambda_1/\lambda_5$	0.5298	0.8656
$\lambda_2/\lambda_5$	0.1897	0.4090
$\lambda_3/\lambda_5$	<b>0.6506</b>	<b>0.9256</b>
$\lambda_4/\lambda_5$	<b>0.7732</b>	<b>0.9249</b>

By considering both sensitivity and linearity, wavelength pairs of  $\lambda_2/\lambda_3$  and  $\lambda_2/\lambda_4$  were selected for further analysis since they provide moderate sensitivity and high linearity. Linearity is important since it determines the sensor accuracy. The transmittance ratio graphs for  $\lambda_2/\lambda_3$  and  $\lambda_2/\lambda_4$  are shown in Figure 1.7. It is shown that the transmittance ratio increased as the refractive index increased. However, as expected, the transmittance at single wavelength, decreased as the refractive index increased. The transmittances at wavelength of  $\lambda_2$ ,  $\lambda_3$ , and  $\lambda_4$  for various refractive index are shown in Figure 1.8. From Figure 1.8, it is also noticed that the single-wavelength methods showed high linearity with correlation factor of above 0.96 as well as high sensitivity. The highest sensitivity and linearity showed at the measurement at  $\lambda_4$ , which are -1.0481/RIU and 0.9851, respectively. Good sensitivity and linearity at single-wavelength method contribute to the high sensitivity and linearity of the dual-wavelength method.



(a)



(b)

**Figure 1.7** Transmittance ratio of the MZI vs. refractive index for (a)  $\lambda_2/\lambda_3$  and (b)  $\lambda_2/\lambda_4$

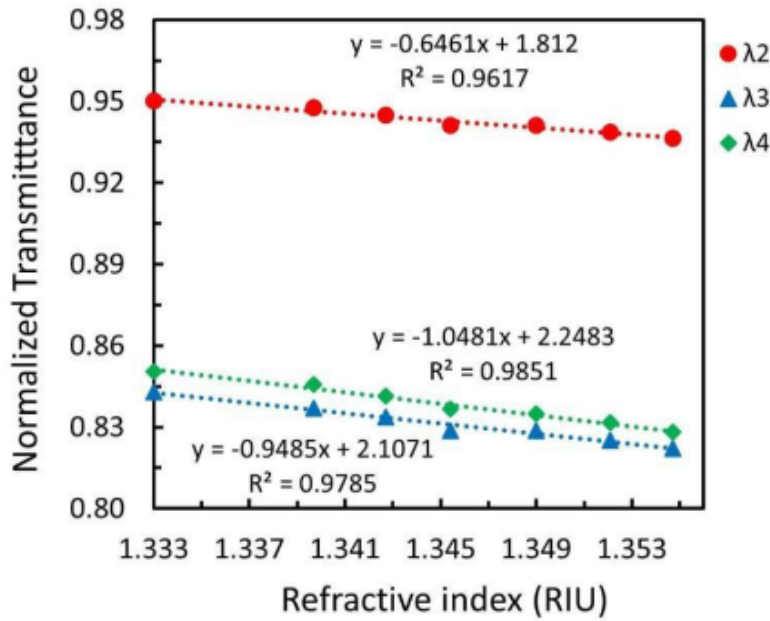


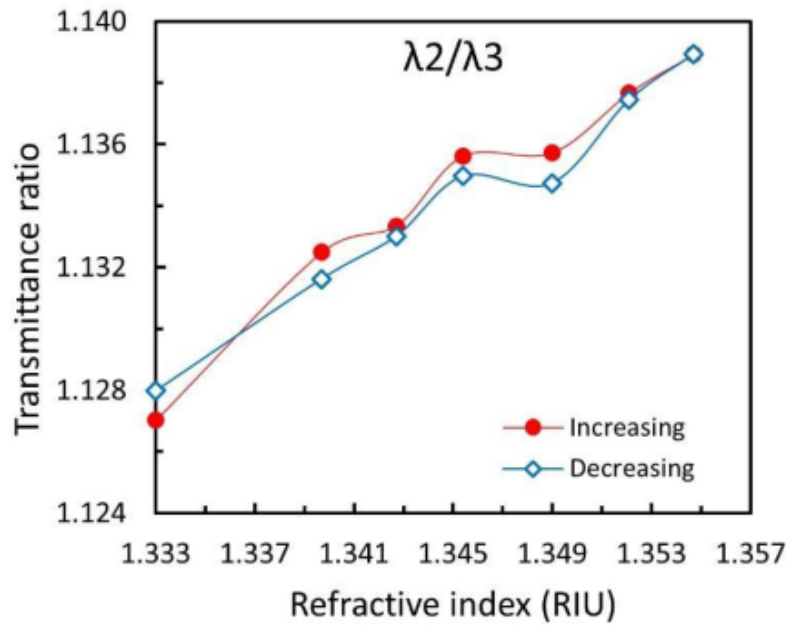
**Figure 18** Normalized transmittance of the MZI vs. refractive index for  $\lambda_2$ ,  $\lambda_3$  and  $\lambda_4$

### 1.4.2 Hysteresis and Accuracy

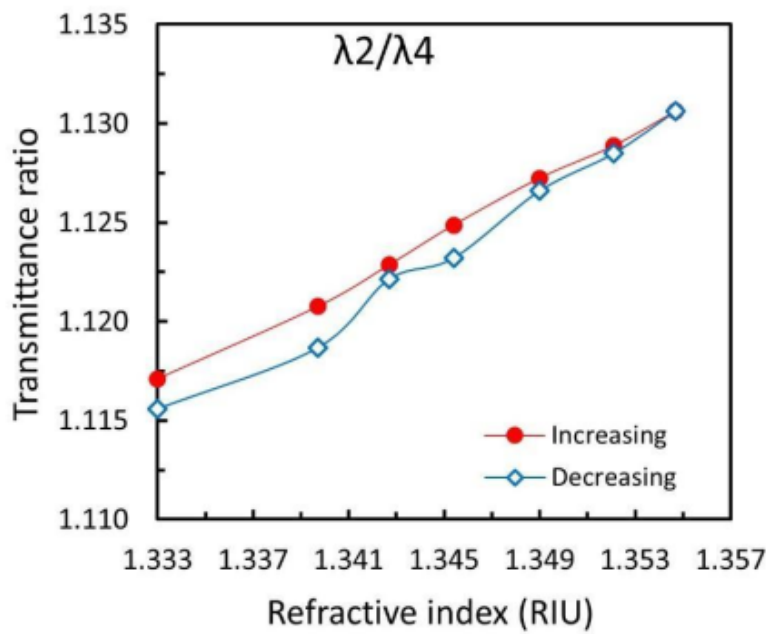
Hysteresis characterization was done by performing reverse measurement from the highest refractive index to the lowest. The results of a full cycle measurement at  $\lambda_2/\lambda_3$  and  $\lambda_2/\lambda_4$  are shown in Figure 1.9. Total hysteresis error ( $H$ ) is the maximum hysteresis error across the full cycle as defined by (Avila-Garcia et al. 2018)

$$H = \left( \frac{I(i) - D(i)}{I(i)} \right) \tag{1.3}$$

where  $I(i)$  and  $D(i)$  are the transmittance ratio from the increasing measurement and the decreasing measurement of the  $i^{th}$  data, respectively. Calculation results showed that  $\lambda_2/\lambda_3$  has lower hysteresis error than  $\lambda_2/\lambda_4$ . The values of the hysteresis error for  $\lambda_2/\lambda_3$  and  $\lambda_2/\lambda_4$  are  $8.67 \cdot 10^{-4}$  and  $1.857 \cdot 10^{-3}$ , respectively. Beside non linearity, hysteresis is another factor that contributes to the sensor accuracy.



(a)



(b)

**Figure 19** Hysteresis curve of dual-wavelength method at (a)  $\lambda_2/\lambda_3$  and (b)  $\lambda_2/\lambda_4$

For comparison, hysteresis of single-wavelength method was also analyzed. Hysteresis of measurement at  $\lambda_4$  was used since it has the highest sensitivity and linearity. The hysteresis curve of measurement at  $\lambda_4$  is shown in Figure 1.10. The total hysteresis obtain from calculation is  $4.212 \cdot 10^{-3}$ . Therefore, the dual-wavelength measurement provides better hysteresis compared to the single-wavelength method. Hysteresis improvement obtained by using wavelength pair of  $\lambda_2/\lambda_3$  and  $\lambda_2/\lambda_4$  are 79.4% and 55.9%, respectively.

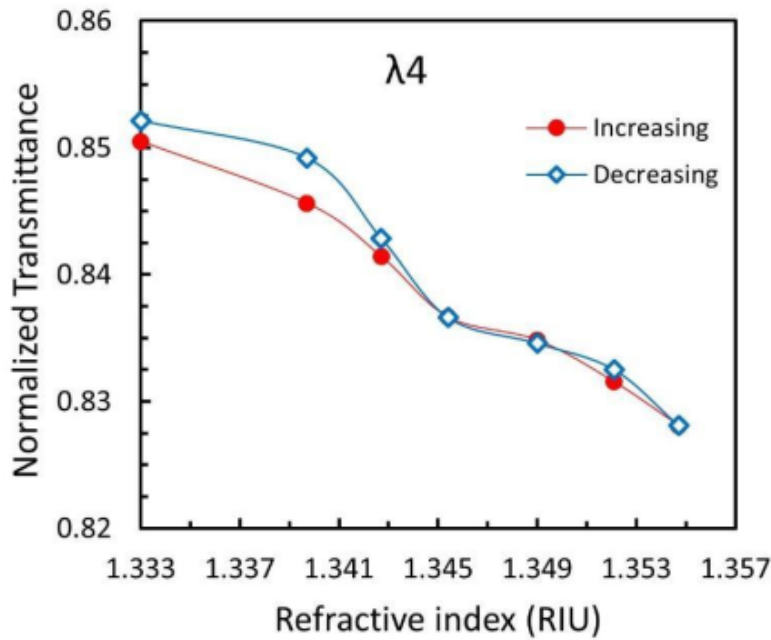


**Figure 1.10** Hysteresis curve of single-wavelength method at  $\lambda_4$

To investigate the accuracy, the refractive index obtained from dual-wavelength methods were calculated using the linear regression equation obtained from graphs in Figure 1.9(a) and (b), as defined by

$$n_1 = \frac{Tr - 0.4415}{0.5151} \quad (1.4)$$

$$n_2 = \frac{Tr-0.2723}{0.6336} \quad (1.5)$$

where  $n_1$  and  $n_2$  are the refractive index obtained using wavelength pair of  $\lambda_2/\lambda_3$  and using wavelength pair of  $\lambda_2/\lambda_4$ , respectively. Whereas  $Tr$  is the transmittance ratio obtained from the measurement. The accuracy is obtained by calculating the relative error of the measured refractive index compared to the actual refractive index (the actual refractive index of the glucose solution measured by using ABBE refractometer). The accuracy of the single-wavelength method was also calculated for comparison purpose. The measured refractive index using wavelength of  $\lambda_4$  ( $n_3$ ) is defined by the regression linear equation obtained in Figure 1.8, which is

$$n_3 = \frac{Tr-2.2483}{1.0481}. \quad (1.6)$$

The relative errors of twice measurement using dual-wavelength and single wavelength method are shown in Figure 1.11. It is shown that, by using single wavelength method, the relative errors of the two cycles are different in significant values. It is indicated that the single wavelength method is highly affected by the transmittance fluctuation during measurement. The highest relative errors of all measurement of the single wavelength method is 0.357%. Meanwhile, for the dual-wavelength method, the highest relative errors are 0.235% and 0.291% for  $\lambda_2/\lambda_3$  and  $\lambda_2/\lambda_4$ , respectively. Therefore, the accuracy improvement of the dual wavelength method are 34.21% and 18.64% for  $\lambda_2/\lambda_3$  and  $\lambda_2/\lambda_4$ , respectively. Clearly, the higher sensor accuracy was achieved by implementing wavelength pair of  $\lambda_2/\lambda_3$ . This result is in line with the result of the hysteresis analysis and it is acceptable since the more hysteresis error is reduced, the higher the accuracy is.



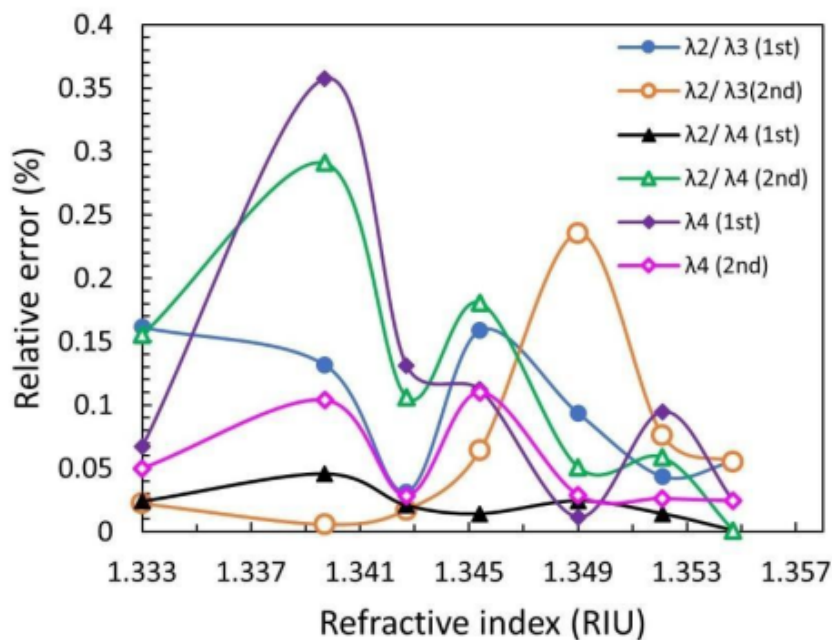


**Figure 1.11** Relative error of dual-wavelength and single-wavelength method for two cycle measurement

## 1.5 CONCLUSION

Intensity-based MZI sensor for refractive index measurement using SI-POF has been fabricated by forming two tapers. The measurement method was done by using dual-wavelength to improve the sensor accuracy. The results showed that by using the proposed dual-wavelength method, the hysteresis error was significantly reduced to 79.4%. As consequence, the sensor accuracy was improved with improvement up to 34.21%. The highest improvement was achieved at wavelength pair of  $\lambda_2/\lambda_3$ .

## ACKNOWLEDGEMENT

2 We would like to thank to Ministry of Education and Culture, Indonesia for funding the research through grant no 19.25.3/UN37/PPK.6.8/2021. Our gratitude also goes to the

3 members of Physics Department, Universitas Negeri Semarang for their helpful discussion throughout the completion of this work.

## REFERENCES

- Avila-Garcia, Maria Susana et al. 2018. "High Sensitivity Strain Sensors Based on Single-Mode-Fiber Core-Offset Mach-Zehnder Interferometers." *Optics and Lasers in Engineering* 107: 202–6.
- Bhardwaj, Vanita, and Vinod Kumar Singh. 2016. "Fabrication and Characterization of Cascaded Tapered Mach-Zehnder Interferometer for Refractive Index Sensing." *Sensors & Actuators: A. Physical* 244: 30–34.
- Chen, Hailiang et al. 2021. "Bubble Microcavity Strain and Gravity Sensor with Temperature and Bending Insensitivity Using an Ultra-Thin Core Optical Fiber." *Optics & Laser Technology* 142: 107193.
- Ghaffar, Abdul et al. 2021. "A Novel Sensor Design for Displacement Measurement Using Plastic Optical Fiber-Based on Face-Coupling Method." *Optical Fiber Technology* 67: 102684.
- Huang, Lin et al. 2020. "Optical Fiber Fabry-Perot Interferometer Refractive Index Sensor Based on Vernier Effect for Silica Colloidal Sol Aging Monitoring." *Optical Fiber Technology* 60: 102338.
- Jasim, A. A. et al. 2014. "Refractive Index and Strain Sensing Using Inline Mach-Zehnder Interferometer Comprising Perfluorinated Graded-Index Plastic Optical Fiber." *Sensors and Actuators, A: Physical* 219: 94–99.
- Li, Wen et al. 2020. "Theoretical Analysis on SPR Based Optical Fiber Refractive Index Sensor with Resonance Wavelength Covering Communication C+L Band." *Optik* 213: 164696.
- Li, Xuefeng et al. 2020. "A New Type of Structure of Optical Fiber Pressure Sensor Based on Polarization Modulation." *Optics and Lasers in Engineering* 130: 106095.

- Melo, Luis, Geoff Burton, Philip Kubik, and Peter Wild. 2016. "Refractive Index Sensor Based on Inline Mach-Zehnder Interferometer Coated with Hafnium Oxide by Atomic Layer Deposition." *Sensors and Actuators, B: Chemical* 236: 537–45.
- Samavati, Zahra et al. 2019. "Comprehensive Investigation of Evanescent Wave Optical Fiber Refractive Index Sensor Coated with ZnO Nanoparticles." *Optical Fiber Technology* 52: 101976.
- Su, Hang et al. 2021. "High-Sensitivity Optical Fiber Temperature Sensor with Cascaded Configuration of MZI and FPI Based on Vernier Effect." *Optical Fiber Technology* 67: 102751.
- Tapetado, A et al. 2014. "Self-Referenced Temperature Sensor Based on a Polymer Optical Fiber." 9157: 12–15.
- Wang, Qi et al. 2016. "High Sensitivity Refractive Index Sensor Based on Splicing Points Tapered SMF-PCF-SMF Structure Mach-Zehnder Mode Interferometer." *Sensors and Actuators, B: Chemical* 225: 213–20.
- Wu, Yongfeng et al. 2021. "Improved Optical Fiber Mach-Zehnder High-Sensitivity Refractive Index Sensor." *Optik* 229: 166214.
- Xu, Yichao, Meng Xiong, and Hui Yan. 2021. "A Portable Optical Fiber Biosensor for the Detection of Zearalenone Based on the Localized Surface Plasmon Resonance." *Sensors and Actuators B: Chemical* 336: 129752.
- Zhang, Zhen et al. 2018. "Groove Micro-Structure Optical Fiber Refractive Index Sensor with Nanoscale Gold Film Based on Surface Plasmon Resonance." *Optical Fiber Technology* 43: 45–48.
- Zheng, Yuanyuan, Xiaozhan Yang, Wenlin Feng, and Wei Fan. 2021. "Optical Fiber Refractive Index Sensor Based on SMF-TCF-NCF-SMF Interference Structure." *Optik* 226: 165900.

# Book chapter

## ORIGINALITY REPORT

15%

SIMILARITY INDEX

10%

INTERNET SOURCES

11%

PUBLICATIONS

3%

STUDENT PAPERS

## PRIMARY SOURCES

1	<a href="http://journal.unesa.ac.id">journal.unesa.ac.id</a> Internet Source	2%
2	Ian Yulianti, N.M. Dharma Putra, Fianti, A.L. Dewi, D. Paradita. "Performances characterization of unsaturated polyester resin/polymethylmethacrylate waveguide for refractive index measurement", Optik, 2021 Publication	1%
3	<a href="http://lib.unnes.ac.id">lib.unnes.ac.id</a> Internet Source	1%
4	"Advanced Photonic Structures for Biological and Chemical Detection", Springer Science and Business Media LLC, 2009 Publication	1%
5	Na Zhang, Wei Xu, Shanhong You, Cheungchuen Yu, Changyuan Yu, Bo Dong, Kunpu Li. "Simultaneous measurement of refractive index, strain and temperature using a tapered structure based on SMF", Optics Communications, 2018 Publication	1%
6	<a href="http://www.frontiersin.org">www.frontiersin.org</a> Internet Source	1%
7	Submitted to University of Southampton Student Paper	<1%
8	Wang, Qi, Lingxin Kong, Yunli Dang, Feng Xia, Yongwei Zhang, Yong Zhao, Haifeng Hu, and Jin Li. "High sensitivity refractive index sensor	<1%

based on splicing points tapered SMF-PCF-SMF structure Mach-Zehnder mode interferometer", Sensors and Actuators B Chemical, 2016.

Publication

9

Dnyandeo Pawar, S.N. Kale. "Birefringence manipulation in tapered polarization-maintaining photonic crystal fiber Mach-Zehnder interferometer for refractive index sensing", Sensors and Actuators A: Physical, 2016

Publication

<1 %

10

Submitted to Universiti Teknikal Malaysia Melaka

Student Paper

<1 %

11

opg.optica.org

Internet Source

<1 %

12

"AETA 2016: Recent Advances in Electrical Engineering and Related Sciences", Springer Science and Business Media LLC, 2017

Publication

<1 %

13

archive.org

Internet Source

<1 %

14

Yanping Xu, Ping Lu, Liang Chen, Xiaoyi Bao. "Recent Developments in Micro-Structured Fiber Optic Sensors", Fibers, 2017

Publication

<1 %

15

patents.google.com

Internet Source

<1 %

16

www.osapublishing.org

Internet Source

<1 %

17

Peng Xue, Fangda Yu, Bingcheng Wu, Haiyang Bao, Jie Zheng. "Investigation of a D-Shaped Plastic Optical Fiber Assisted by a Long Period

<1 %

# Grating for Refractive Index Sensing", IEEE Sensors Journal, 2020

Publication

18

Yongfeng Wu, Bo Liu, Tong Nan, Jing Wu, Yaya Mao, Jianxin Ren, Lilong Zhao, Tingting Sun, Jin Wang, Yang Han, Yulan Zhang. "Improved optical fiber Mach-Zehnder high-sensitivity refractive index sensor", Optik, 2020

Publication

<1 %

19

[ilps.uobaghdad.edu.iq](http://ilps.uobaghdad.edu.iq)

Internet Source

<1 %

20

[www.jas.shu.edu.cn](http://www.jas.shu.edu.cn)

Internet Source

<1 %

21

Abdul Ghaffar, Qi Li, Mujahid Mehdi, Bhagwan Das, Ishrat Hameed Alvi, Qifeng Xie, Jiyuan Ma. "Multiplexing Sensors Technique for Angle and Temperature Measurement Using Polymer Optical Fiber", Infrared Physics & Technology, 2023

Publication

<1 %

22

Daniele Tosi, Marzhan Sypabekova, Aliya Bekmurzayeva, Carlo Molardi, Kanat Dukenbayev. "Interferometers", Elsevier BV, 2022

Publication

<1 %

23

Lina Dong, Ge Chen, Guangyang Liu, Xiaodong Huang et al. " A review on recent advances in the applications of composite Fe O magnetic nanoparticles in the food industry ", Critical Reviews in Food Science and Nutrition, 2022

Publication

<1 %

24

Submitted to Multimedia University

Student Paper

<1 %

25

[research.library.mun.ca](http://research.library.mun.ca)

Internet Source

<1 %

26 [www.ablesci.com](http://www.ablesci.com) Internet Source <1 %

---

27 [www.mdpi.com](http://www.mdpi.com) Internet Source <1 %

---

28 [www.science.gov](http://www.science.gov) Internet Source <1 %

---

29 Carlos A. J. Gouveia, Jose M., Pedro A.S.. "Chapter 13 Refractometric Optical Fiber Platforms for Label Free Sensing", IntechOpen, 2013  
Publication <1 %

---

30 G. Salceda-Delgado, A. Martinez-Rios, I. Torres-Gomez, G. Anzueto-Sanchez, T.E. Porraz-Culebro. "Experimental analysis for refractive index sensing by using a compact, simple and robust Mach-Zehnder interferometer based on an air gap inside of a fiber", Optical Fiber Technology, 2022  
Publication <1 %

---

31 "Computational Photonic Sensors", Springer Science and Business Media LLC, 2019  
Publication <1 %

---

32 Vanita Bhardwaj, Kamal Kishor, Avinash C. Sharma. "Tapered optical fiber geometries and sensing applications based on Mach-Zehnder Interferometer: A review", Optical Fiber Technology, 2020  
Publication <1 %

---

Exclude quotes On

Exclude matches < 4 words

Exclude bibliography On

# Book chapter

GRADEMARK REPORT

FINAL GRADE

**/0**

GENERAL COMMENTS

**Instructor**

PAGE 1

PAGE 2

PAGE 3

PAGE 4

PAGE 5

PAGE 6

PAGE 7

PAGE 8

PAGE 9

PAGE 10

PAGE 11

PAGE 12

PAGE 13

PAGE 14

PAGE 15

PAGE 16

PAGE 17

PAGE 18